Kaon Production on the Deuteron Using Polarized Photons

P. Nadel-Turoński[1,2], B.L. Berman[2], C. Bennhold,
G. Feldman, Y. Ilieva, A. Tkabladze, A. Waluyo
The George Washington University, Washington, DC 20052

F.J. Klein, J. Santoro
The Catholic University of America, Washington, DC 20064

E. Pasyuk
Arizona State University, Tempe, AZ 85287

D. Ireland, K. Livingston
University of Glasgow, Glasgow G12 8QQ, United Kingdom

L. Guo, J.-M. Laget, S. Stepanyan
Thomas Jefferson National Accelerator Facility, Newport News, VA 23606

December 5, 2005

[1]Contact Person: turonski@jlab.org
[2]Intended Co-Spokespersons (to date)

Abstract

This letter of intent proposes a CLAS experiment to measure kaon photoproduction using circularly and linearly polarized photon beams and a liquid deuterium target. The self-analyzing nature of Λ and Σ hyperons allows measurement of both single and double polarization observables (8 out of 16 possible), at a high rate and with low background. The primary purpose is to study strange decays of N^* states photoproduced on the neutron in search of "missing" resonances, and the interaction of nucleons with polarized hyperons. The former will provide strong constraints for the new coupled-channel calculations aimed at resolving the ambiguities inherent in previous approaches, and the possibility to study resonances that have large neutron helicity amplitudes but may not be prominent in proton data. The $K^0\vec{\Lambda}$ channel is also predicted to be particularly sensitive to the much-debated "missing" $D_{13}(1900)$ resonance. For final-state interactions, polarization observables are sensitive to the predictions of different $\vec{Y}-N$ interaction potentials, and can determine the contributions from various partial waves. At higher energies, they provide input for the development of rescattering models that are necessary for the understanding of color transparency. No new hardware is needed for this experiment, and it is very flexible in terms of the required beam energies and polarizations, making it easy to schedule. The general nature of the setup will allow it to run concurrently with other deuterium experiments in CLAS, and the data can also be used for a wide range of analyses that are not included in the current proposal.

1 Introduction and Motivation

Understanding the structure of the nucleon is a major goal of the research program at Jefferson Lab. Measurement of the spectrum of excited baryons and their decay amplitudes is an important part of this effort. Of particular interest is the search for "missing" resonances, predicted by the SU(6) $\times$ O(3) symmetry of constituent quark models [1], but not found experimentally. In contrast, they do not appear in di-quark models [2], which have fewer degrees of freedom. It is thus essential to establish whether the difficulty in finding the "missing" states truly reflects the presence of a strongly correlated quark pair inside the nucleon. To distinguish between the two cases, one does not need to find all of the states in the "missing" multiplets. A few clear observations from different multiplets that are incompatible with the di-quark model predictions would suffice.

In recent years, there have been two major developments in N^* physics. On the theory side, coupled-channel analyses [3, 4], which include pion, eta, and kaon production, have appeared and show a lot of promise in resolving the ambiguities present when the resonance parameters are extracted from partial wave analysis or from earlier (isobaric) models [5, 6, 7, 8, 9, 10, 11]. Within the coupled-channels framework, data of reasonable quality in many channels provide a better constraint than precise data in only a few. This makes it imperative not only to focus on pion photoproduction on the proton, but also to investigate the weaker N^* decay channels. The strange decays in particular offer a possibility to find resonances that do not couple strongly to pions [12, 13].

Measurement of polarization observables in high-statistics experiments provides another way of constraining the models. At Jefferson Lab, the success of the g8b experiment, which used linearly polarized photons [14], demonstrated a new capability. And the importance of polarization measurements in strangeness photoproduction, as part of the search for missing

nucleon resonances, has already been recognized by the PAC, as shown by the A- rating for experiment E-02-112 [15].

Both of the experiments mentioned above use proton targets, but data are also needed for the neutron channels. This letter thus proposes an experiment that uses polarized photon beams and a liquid deuterium target. For an exclusive measurement, the hyperon recoil polarization (P) gives access to polarization-transfer observables ($C_{x'}, C_{z'}, O_{x'}, O_{z'}$), and to the beam asymmetry (Σ). Using a linearly polarized beam and measuring the recoil polarization further allows for a measurement of the target asymmetry (T).

$$\begin{aligned} \frac{d\sigma}{d\Omega} &= \sigma_0 \{1 - P_{lin}\Sigma \cos 2\varphi \\ &\quad + P_{x'} \left(-P_{lin} O_{x'} \sin 2\varphi - P_\lambda C_{x'}\right) \\ &\quad - P_{y'} \left(-P + P_{lin} T \cos 2\varphi\right) \\ &\quad - P_{z'} \left(P_T O_{z'} \sin 2\varphi + P_\lambda C_{z'}\right) .\} \end{aligned} \tag{1}$$

In addition, more statistics will reduce the uncertainties in the determination of the differential cross sections. It may be interesting to obtain additional polarization observables using an HD or frozen-spin target (FROST), but for the above mentioned ones a clean experiment is clearly preferable. Not only can the required statistics be obtained much faster by using a longer, undiluted target (this is particularly important for linear photon polarization when the rate is limited by the tagger), but also by having less overhead during the experiment. More importantly, the systematic uncertainties would be smaller by avoiding complications with the deuteron tensor polarization contribution and backgrounds from both the target cell and target material; a thorough Understanding the latter is especially important for the deuterated butanol of the frozen-spin target. The cryostat of the BNL HD target, on the other hand, would have to be modified for the use in CLAS. Should this be successful, the target would still not be available for experiments until 2008.

The most urgent requirement of the current coupled-channel analyses is data on the elementary processes, *i.e.*, $\gamma n \to K^0\Lambda$, $\gamma n \to K^0\Sigma^0$, and $\gamma n \to K^+\Sigma^-$. The latter two are necessary to constrain the corresponding proton channels [16]. Also, with the current proton data, the Giessen [3] and GW [4] coupled-channel analyses disagree with respect to the existence of the "missing" $D_{13}(1900)$ resonance [17, 18]. The former group sees the enhancement as a coherent sum of resonance and background contributions [19]. Earlier, Saghai argued that the structure at $W = \sqrt{s} = 1.9$ GeV could be reproduced without the $D_{13}(1900)$ resonance by taking into account off-shell effects [20], while Janssen *et al.* saw an improvement in the description of the $\gamma p \to K^+\Lambda$ data by inclusion of the $D_{13}(1900)$, but did not rule out alternative interpretations [10]. It is interesting to note that the properties of the $D_{13}(1900)$ resonance, present in the GW calculations, seem to be very sensitive to the $\gamma n \to K^0\Lambda$ channel, making it both difficult to predict and interesting to measure. There are also some known resonances, such as the $D_{15}(1675)$, that have neutron helicity amplitudes that are significantly larger than those for the proton [21]. The same can be true for some "missing" ones. In both cases, neutron data can lead to a better understanding.

Going beyond the elementary amplitudes, substantial partial N^* decay widths are predicted for strange channels where either the kaon or the hyperon is in an excited state [12]. These channels will eventually have to be included in a complete model. Right now there are no neutorn data, but we hope to remedy this by measuring production of the low-lying K^* and Y^* final states. Knowing the properties of the latter also has important merits of its own. Potential models predict, for example, the spin-$\frac{3}{2}$ $\Lambda(1520)$ to be nearly degenerate with its spin-$\frac{1}{2}$ partner, the $\Lambda(1405)$. A possible explanation for the large mass difference is that the latter is a "molecular" $\bar{K}N$ bound state. Since similar descriptions have been suggested for N^* states, studies of Λ^* decays can have important implications for them as well.

Finally, the deuteron is the simplest possible system for the study of final-state interactions [22, 23, 24]. A good description of such processes is clearly required for analysis of the quasi free case. The importance of rescattering models does, however, go well beyond this. A recent example is the question of color transparency [25]. It is predicted that a high-t reaction can cause the two quarks in a meson to assume a point-like configuration, for which a strongly interacting medium will be transparent, but the relaxation time is short, typically as long as it takes for the meson to traverse the radius of a nucleon. In order to observe the predicted drop in the cross section at high t, the scattering target thus has to be very close to the production point. At the proposed energies it will not be possible to observe the onset of color transparency, but such data are required to calibrate the model in order to make reliable predictions for high t. This approach has also recently led to the first direct observation of $\Sigma^-(1385)$ scattering on the proton [26], but better statistics are needed.

In addition to polarization transfer, measurement of the recoil polarization makes it possible to study the $\vec{Y} - N$ final-state interaction. Recent calculations show the sensitivity of polarization observables to the properties of various modern interaction potentials [27]. The presently proposed scattering experiment would thus be complementary to bound-state hypernuclear experiments that currently comprise an important part of the program at Jefferson Lab [28].

2 Previous Experiments

There are currently no published strangeness photoproduction data on the deuteron, polarized or not. This section will therefore discuss other experiments that show a relevant degree of similarity.

On the proton there are several published results, notably by the SAPHIR [29, 30] and CLAS [31, 32] collaborations - the latter from the E-89-004 [33] experiment, using the g1

data set.

For the deuteron, there are two real-photon data sets from CLAS: g2 and g10. One of the four approved experiments from the former run period, and the only one dealing with strangeness, was E-89-045 [34]. It envisaged inclusive and exclusive measurements of the cross sections for the six elementary strangeness production channels on the nucleon

$\gamma p \to K^+\Lambda$
$\gamma p \to K^+\Sigma^0$
$\gamma p \to K^0\Sigma^+$
$\gamma n \to K^0\Lambda$
$\gamma n \to K^0\Sigma^0$
$\gamma n \to K^+\Sigma^-$

as well as the investigation of the hyperon-nucleon interaction.

There are inclusive [35] and exclusive [36] cross section analyses in progress for the $K^+\Sigma^-$ channel using the g2 data. The recent high-statistics (10 billion triggers) g10 experiment [37], has also made it possible to perform exclusive analyses [38] of the two remaining neutron channels, aimed at extracting both the differential cross sections and the recoil polarization.

Unfortunately, neither of these two data sets allows further polarization studies. In the case of g2, which did use a circularly polarized photon beam, the main obstacle is the insufficient statistics. Today, progress in operation of the accelerator allows higher electron-beam polarization (up to 80%), which translates into higher (circular) photon polarization. During the g10 run period, however, a polarized beam was not requested and was not delivered.

For linearly polarized beams, there are currently no CLAS data on the deuteron. The recent g8b run did, however, clearly demonstrate the capabilities of the coherent-bremsstrahlung facility in Hall B, reaching 92% linear polarization with the coherent photon peak at 1.3 GeV. In this kind of experiment the capability of CEBAF and CLAS are unique. No other laboratory offers a comparable combination of energy, luminosity, polarization, and charged-particle acceptance that is required for exclusive measurements. Thus, there will be no other data

forthcoming in the foreseeable future that can answer the physics questions posed in this letter.

To give a short overview of other facilities, GRAAL in Grenoble and MAMI in Mainz, the latter even after the planned upgrade, both have beam energies up to only 1.5 GeV, which will be barely at threshold for the $D_{13}(1900)$, as well as for K^* and Y^* final states.

The ELSA facility in Bonn [39] uses the same coherent-bremsstrahlung method to produce linearly polarized beams that is employed at JLab, but its maximum electron energy is considerably lower (nominally 3.5 GeV, compared with 6 GeV). Since the degree of linear photon polarization increases with the ratio of E_e/E_γ, the facility in Hall B is significantly better for higher photon energies. More importantly, the current detector configuration at ELSA is intended for neutral particles, and can therefore be seen at best as complementary to CLAS.

LEPS at Spring-8 [40] has highly polarized beams (up to 2.4 GeV, using a 351 nm laser); recently, beam polarization asymmetries for the $\vec{\gamma}p \to K^+\Lambda$ and $\vec{\gamma}p \to K^+\Sigma^0$ channels were published [41], and $\vec{\gamma}d$ data are being analyzed as part of the search for pentaquark states. In contrast to CLAS, however, the detector acceptance is limited to very forward angles, and is thus not well suited for the exclusive measurements proposed in this letter.

3 Theoretical Underpinnings and Experimental Feasibility

3.1 N^* decays to $K\vec{\Lambda}$ and $K\vec{\Sigma}$

3.1.1 Theory

Baryon resonances are identified by their quantum numbers, such as orbital angular momentum, spin, isospin, and parity. These quantum numbers correspond to the partial waves

where the baryon resonances are excited. According to their appearance in each partial wave, baryon resonances are categorized as first-tier, second-tier, and third-tier. An example of this are the $D_{13}(1520)$, $D_{13}(1700)$, and $D_{13}(2080)$ resonances listed by the Particle Data Group (PDG) [42]. In most cases, the extraction of first-tier resonance properties, such as mass, decay-width, and helicity amplitudes, are in agreement with each other to within 20%. In contrast, only rough agreement is found for the mass of a second-tier resonance in each partial wave. Decay widths and helicity amplitudes vary widely in most cases. The situation is even worse for the third-tier resonances.

As part of the effort to investigate the baryon resonances, Waluyo and Bennhold have made significant progress in developing a new coupled-channels, "Chiral-Symmetry-Inspired" (CSI) model [4]. It is based on the work by Feuster and Mosel [43], but the driving terms of the original model, which are defined through traditional effective Lagrangians, have been replaced by ones with new background and resonance parts. The new background consists of a potential that takes into account the requirements of $SU(3)$ chiral dynamics. This involves expanding the chiral Lagrangian to a given order, and includes contact terms permitted to that order. At the same time, the resonance contributions have been updated using the modern covariant resonance Lagrangians derived by Pascalutsa. This fixes the incorrect spin degree of freedom and discards the ambiguous off-shell terms inherent in the old Rarita-Schwinger types of Lagrangians.

Having these modifications in place, new background amplitudes are reconstructed from the standard s-, u- and t- Born terms, σ and a_0 scalar-meson resonances,, ρ, ω, and K^* vector-meson resonances, as well as Weinberg-Tomozawa and higher-order chiral contact terms. The new resonance amplitudes are constructed from the s- and u-channel pole diagrams where spin-$\frac{1}{2}, \frac{3}{2}$, and $\frac{5}{2}$ baryon resonances propagate in the intermediate states. This is the first coupled-channels model where baryon resonances are included using modern hadronic and electromagnetic interaction Lagrangians.

In general, the CSI model comprises five asymptotic states of $\pi N, 2\pi N, \eta N, K\Lambda$, and

$K\Sigma$. The 2π system is approximated using the scalar-isovector ζ particle. The Bethe-Salpeter equation is solved in the K-matrix approximation. To ensure that the CSI model is gauge-invariant, the gauge-invariance restoration scheme of Davidson and Workman [44] is implemented. The model is used to investigate baryon resonance states through meson hadro- and photoproduction reactions, and is implemented in the energy region of $W < 2$ GeV. The investigation is focused on the interpretation of the most recent high-quality photoproduction data provided by the CLAS collaboration [45, 46, 31].

In the search for missing resonances, four possible resonance states have been investigated in the energy range of 1.8 - 2.0 GeV. They are the S_{11}, P_{11}, P_{13}, and D_{13}, all of which are the third states in their respective partial wave. Of these, only the D_{13} state has been found, with a mass of 1961 MeV and a total width of 313 MeV. Its properties, and a comparison with the values from other analyses, are shown in Tables 1 and 2. The quality of the fit to the $K\Lambda$ differential cross data [46, 31] at high energies is shown in Fig. 1.

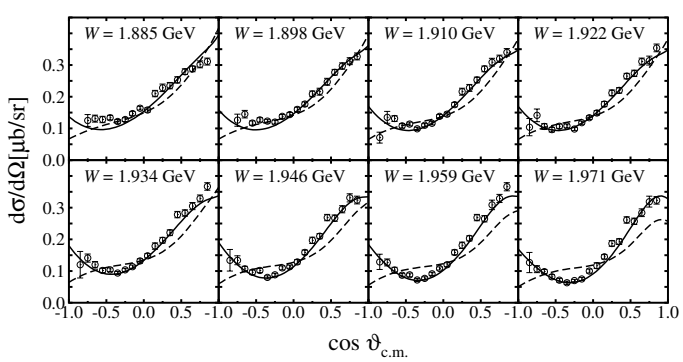

Figure 1: Differential cross section for $\gamma N \to K\Lambda$ at high energies given as function of the kaon angle. The solid and dashed lines show the calculation using the CSI model with and without the $D_{13}(1900)$ resonance.

If it is confirmed, the $D_{13}(1900)$ missing resonance would fall into the PDG [42] 2-star category, where a resonance state is found in different analyses with rough agreement of mass values, but with disagreement with respect to other properties, such as decay width and helicity amplitudes. This, too, is shown in Tables 1 and 2.

$L_{2I,2S}$	Mass	Γ_{tot}	$\beta_{\pi N}$	$\beta_{2\pi N}$	$\beta_{\eta N}$	$\beta_{K\Lambda}$	$\beta_{K\Sigma}$
$D_{13}(1900)$	1961	313	7	48	0.5	15	31
missing	1946(1)	859(7)	12(2)	59(8)	7(2)	0.2(0.2)	0.7(0.4)
	1940	412	10	75	14	0	–

Table 1: Extracted baryon resonance properties in the first and second resonance region (1st line) compared with values taken from Penner *et al.* [3] (2nd line) and Vrana *et al.* [47] (3rd line). The mass and total width are given in MeV, and the decay ratios β are in %.

$L_{2I,2S}$	$A^p_{1/2}$	$A^p_{3/2}$	$A^n_{1/2}$	$A^n_{3/2}$
$D_{13}(1900)$	+21	−1	+130	+123
missing	+12	−10	+23	−9

Table 2: Extracted electromagnetic helicity amplitudes in 10^{-3} GeV$^{-1/2}$ for baryon resonances in the first and second resonance region, compared with values taken from Penner *et al.* [3] (2nd line). The superscript p or n indicates the proton or neutron helicity amplitude.

Until now, the evidence for the $D_{13}(1900)$ comes from the available $K\Lambda$ and $K\Sigma$ photoproduction differential cross section on the proton [46, 31, 29]. Although current coupled-channel analyses [4, 3] give a fairly good description of the $K\Lambda$ and $K\Sigma$ photoproduction data on the proton, most of the extracted properties of the missing $D_{13}(1900)$ resonance vary widely. This is a strong indication that new data are needed to provide more stringent constraints for the extraction of the $D_{13}(1900)$ resonance properties. A careful look at the extracted helicity amplitudes of the $D_{13}(1900)$ resonance, shown in Table 2, suggests which new data sets are needed. The values of $A^n_{\frac{1}{2}}$ and $A^n_{\frac{3}{2}}$ are large, indicating a large sensitivity to the $D_{13}(1900)$ present in the neutron channel of $K\Lambda$ photoproduction, namely, the $\vec{\gamma}n \to K^0\Lambda$ reaction.

From a theoretical point of view, polarization observables provide an advantage over the differential cross section for projecting out the role of a baryon resonance in a specific channel, since they contain interferences of electromagnetic multipoles. For example, the double-polarization observables $O_{x'}$ and $O_{z'}$ can be written in terms of the helicity amplitudes

for meson photoproduction H_1, H_2, H_3, and H_4:

$$O_{x'} = \frac{\mathrm{Im}[H_1^* H_2 - H_3^* H_4]}{\frac{1}{2}(|H_1|^2 + |H_2|^2 + |H_3|^2 + |H_4|^2)}, \tag{2}$$

$$O_{z'} = \frac{\mathrm{Im}[-H_1^* H_4 + H_2^* H_3]}{\frac{1}{2}(|H_1|^2 + |H_2|^2 + |H_3|^2 + |H_4|^2).} \tag{3}$$

The helicity amplitudes can in turn be expressed in terms of CGLN amplitudes [48]:

$$\begin{aligned} H_1 &= \frac{-1}{\sqrt{2}} \sin\theta (F_3 + F_4 \cos\theta), \\ H_2 &= \frac{-1}{\sqrt{2}} (2F_1 - 2F_2 \cos\theta + F_4 \sin^2\theta), \\ H_3 &= \frac{-1}{\sqrt{2}} F_4 \sin^2\theta, \\ H_4 &= \frac{1}{\sqrt{2}} (2F_2 + F_3 + F_4 \cos\theta). \end{aligned} \tag{4}$$

The CGLN amplitudes can, in turn, be expanded in terms of electromagnetic multipoles:

$$\begin{aligned} F_1 &= \sum_{l \leq 0} \{(M_{l+} + E_{l+}) P'_{l+1} + [(l+1) M_{l-} + E_{l-}] P'_{l-1}\}, \\ F_2 &= \sum_{l \leq 1} [(l+1) M_{l+} + l E_{l-}] P'_l, \\ F_3 &= \sum_{l \leq 1} [(E_{l+} - M_{l+}) P"_{l+1} + (E_{l-} + M_{l-}] P"_{l-1}]\}, \\ F_4 &= \sum_{l \leq 2} (M_{l+} - E_{l+} - M_{l-} - E_{l-}) P"_l. \end{aligned} \tag{5}$$

To show the sensitivity of polarization observables to the presence of the $D_{13}(1900)$ resonance, the predictions of the CSI model for $O_{x'}$ and $O_{z'}$ are given in Figs. 2 and 3. These two figures demonstrate how important new polarization data in the neutron channel are for projecting out missing resonances such as the $D_{13}(1900)$.

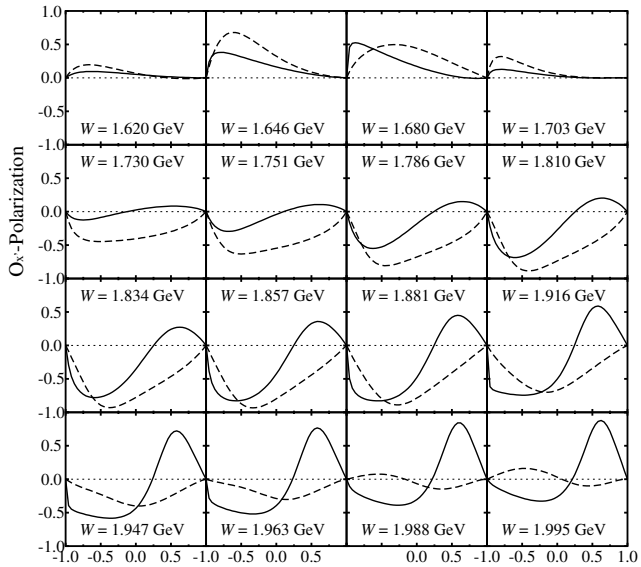

Figure 2: The double polarization observable $O_{x'}$ plotted as a function of $\cos\Theta_K^{c.m.}$ for the $\vec{\gamma}n \to K^0\Lambda$ reaction. The solid and dashed lines show the prediction of the CSI model with and without the missing $D_{13}(1900)$ resonance.

3.1.2 Experiment

The photon polarization will allow us to extract new observables, but the basic challenges of the analysis will not differ much from the exclusive cross section measurements of the $\vec{\gamma}n \to K^0\Lambda, \vec{\gamma}n \to K^0\Sigma^0$, and $\vec{\gamma}n \to K^+\Sigma^-$ channels. We thus have a good handle on channel selection and identification of the quasi free events. The analysis of the $K^+\Sigma^-$ channel requires the detection of the K^+, π^-, and neutron, the latter in the electromagnetic calorimeter. It has already resulted in a CLAS analysis note [36]. The K^0 channels on the neutron are now being analyzed using the low-field (4.71 billion trigger) part of the g10 data set [38].

In the latter analysis, the charged decays of $K_s^0 \to \pi^+\pi^-$ and $\Lambda \to p\pi^-$ are identified by invariant mass, with all four final-state particles being detected in CLAS. This is shown in Fig. 4. These events also include the Σ^0, which decays into $\Lambda\gamma$ (with a branching ratio of

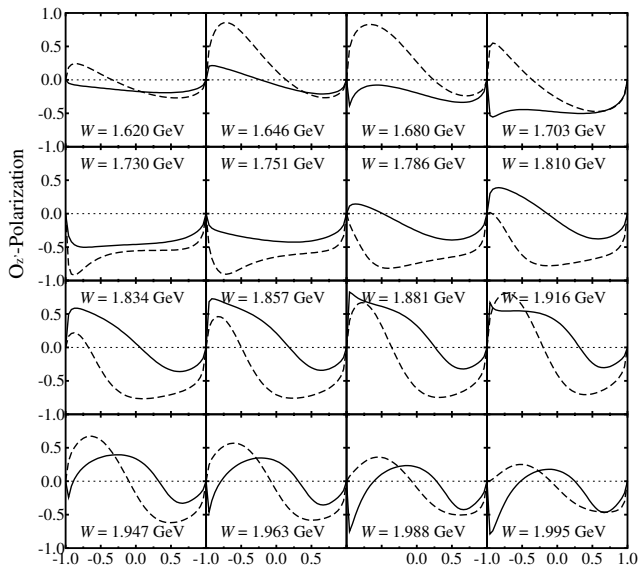

Figure 3: The double polarization observable $O_{z'}$ plotted as a function of $\cos\Theta_K^{c.m.}$ for the $\vec{\gamma}n \to K^0\Lambda$ reaction. The solid and dashed lines show the prediction of the CSI model with and without the missing $D_{13}(1900)$ resonance.

100%).

The quality of the event selection and vertex reconstruction can be judged by how well the K^0 and Λ lifetimes are reproduced. Looking at the fits in Fig. 5, one finds that $\lambda_{K_s^0} = \frac{1}{\tau} = 11.2$ ns^{-1} matches the PDG value [42], while $\lambda_\Lambda = 3.7$ ns^{-1} is very close to the 3.8 ns^{-1} given by the PDG.

For a proton target, the Λ can be separated from the Σ using the kaon missing mass, but owing to Fermi motion this is no longer the case for deuterium. However, by combining the kaon missing mass, as it would appear in an inclusive measurement, with the missing mass of $K^0\Lambda$, one can see the two peaks clearly separated, as shown in Fig. 6. The projections on the $K^0\Lambda$-axis show that there is little background. A simple double-Gaussian fit gives a good description of the mm($K^0\Lambda$) distribution. In total, there are about 30,000 $K^0\Lambda$ and 20,000 $K^0\Sigma^0$ events in the low torus field part of g10. This can serve as a guideline for the circularly proposed experiment. The tail under the Λ peak is small and can be determined with good

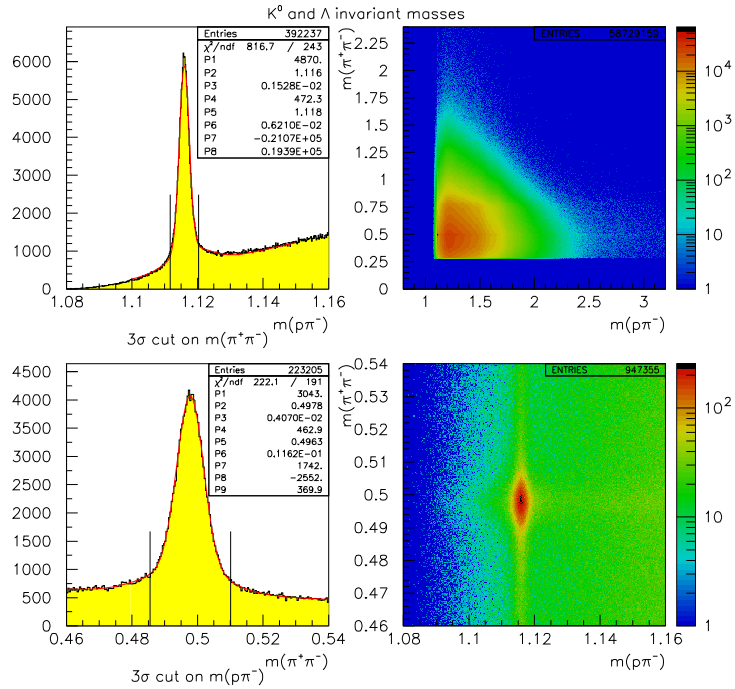

Figure 4: K_s^0 and Λ invariant masses from the low torus field part of g10. Only particle id cuts have been applied. Missing mass cuts significantly reduce the background. Note the logarithmic z-axis on the right.

accuracy. The cross section for the Σ^0 channel can thus be measured simultaneously without requiring that the γ from its decay be detected in the electromagnetic calorimeter, which would significantly reduce the acceptance. Figure 6 also shows that in a subset containing at least half of the data, there is no Σ^0 contribution.

Quasifree production can be selected using the momentum of the reconstructed spectator proton. As shown in Fig. 7, the angular distribution of the spectators is almost isotropic below 0.3 GeV/c, which is also the CLAS detection threshold.

The raw $K^0\Lambda$ and $K^0\Sigma^0$ yields are shown in Fig. 8. Although corrections for acceptance and photon flux can change the shape of this spectrum significantly, this figure shows how the events are distributed. A lower photon energy, 3 GeV instead of the 3.6 GeV in g10, may alter the shape somewhat, but the distribution still provides us with a good guideline for what statistics we can expect.

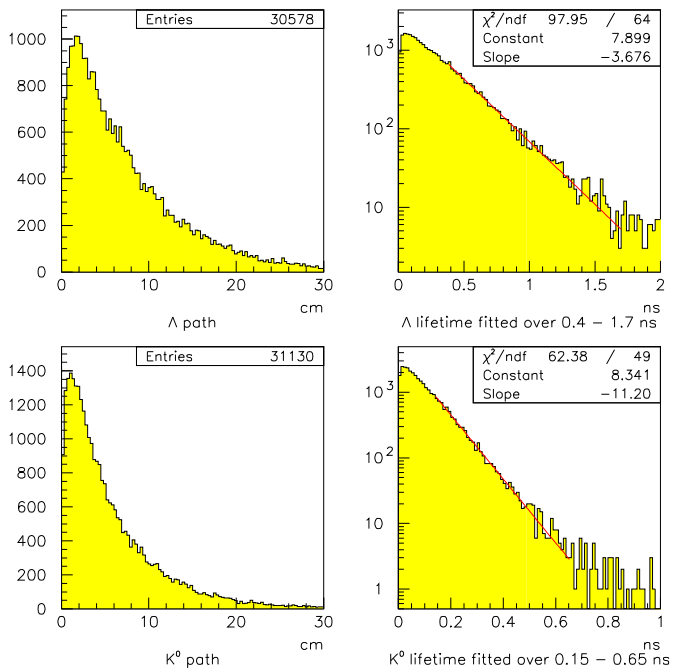

Figure 5: K_s^0 and Λ paths and lifetimes. As expected from the CLAS resolution, there is a slight deficit of events with short path lengths. The agreement of the fit with the PDG values [42], 11.2 ns^{-1} for the K_s^0 and 3.8 ns^{-1} for the Λ, is very good, indicating a satisfactory event selection and vertex reconstruction.

3.2 N^* decays to $K^*\vec{Y}$ and $K\vec{Y}^*$

So far, coupled-channel analyses for N^* physics have mostly been performed by using pion, eta, and kaon production. In the future, more constraints can be added by including K^*Y and KY^* production. A study of N^* decays by Capstick and Roberts [12], using a quark-pair creation model, has predicted that some low-lying negative-parity states, including several missing nucleon resonances, could couple strongly to the K^*Y and KY^* channels. There are several ongoing analyses using existing CLAS g10 and g11 data, investigating the $\gamma p \to K^{*+}\Lambda, \gamma p \to K^{*0}\Sigma^+, \gamma p \to K^+\Sigma^0(1385)$, and $\gamma n \to K^+\Sigma^-(1385) \to K^+\pi^-\Lambda \to K^+\pi^-\pi^-p$ channels. The final state of the latter is well suited for exclusive measurements in CLAS, and the current analysis [38] aims at obtaining the hyperon recoil polarization (P) as well as the cross section. Since neither g10 nor g11 used polarized photons, no other polarization

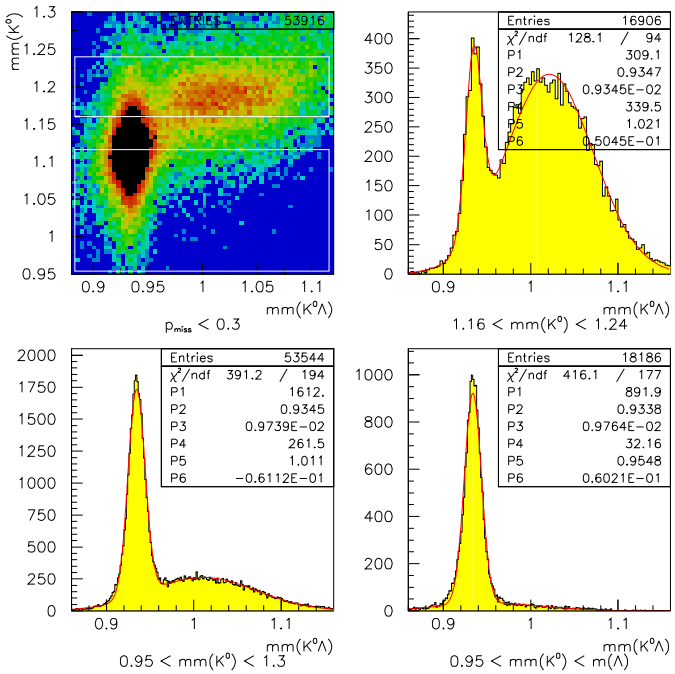

Figure 6: A good $\Lambda - \Sigma^0$ separation can be achieved using the missing mass of the kaon (the hyperon mass) and $K_s^0\Lambda$ (the spectator proton mass). An undetected γ from Σ^0 decay makes the latter distribution broader, peaking to the right of the Λ (top left). The projection (bottom left) shows that the data are well described by a double Gaussian fit. There is very little background. On the right are projection for two mm(K^0) ranges indicated in the top right panel, the lower showing that a clean Λ signal can be extracted with a reasonable loss in statistics.

observables can be determined.

The analysis of the proton channels already has resulted in preliminary total cross sections [49]. In Fig. 9 these are compared with previous measurements for the $K^+\Sigma^0(1385)$ and $K^+\Lambda$ channels [32]. The systematic uncertainty due to normalization and model dependence of yield extraction is estimated to be about 20%. The KY^* and K^*Y cross sections do not seem to be negligible compared with the $K^+\Lambda$ channel, which indicates that these channels should be incorporated into future coupled-channels analyses. These preliminary results also can serve as a guide for what statistics to expect in the presently proposed polarized-photon experiment on the deuteron. Although no theoretical calculation is yet available for the sensitivity of polarization observables to the nucleon resonances for the K^*Y and KY^* channels,

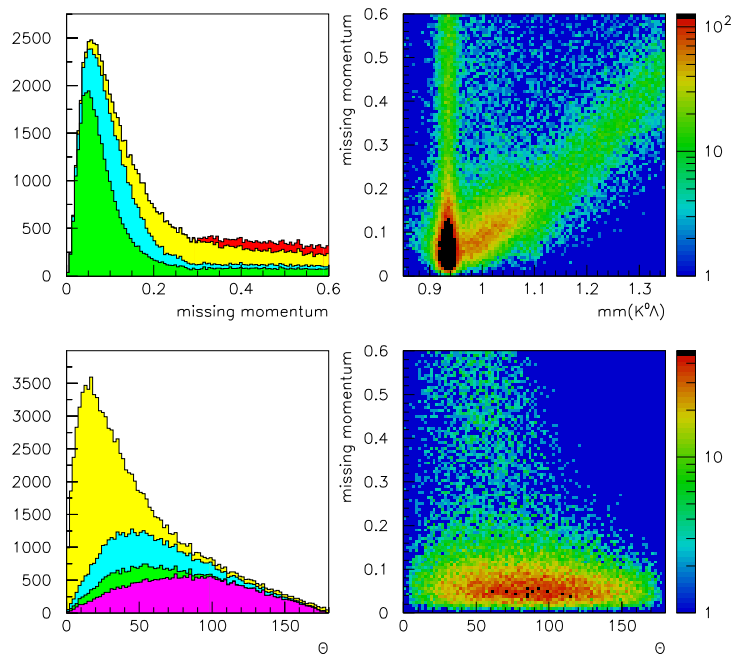

Figure 7: Spectator proton selection. Color coding on the left: exclusive $K^0\Lambda$ (green), ditto with $p_{missing} < 0.3$ GeV (magenta, lower panel), $K^0\Sigma^0$ (blue), and inclusive $K^0\Lambda$ with 1 proton detected and the spectator reconstructed (yellow) and with both protons detected (red, upper panel). Top left: missing (proton) momentum. Bottom left: Spectator proton angular distribution. As expected for true spectators, the distribution for low-momentum protons is isotropic for exclusive $K^0\Lambda$ events. The undetected photon emitted from forward-moving Σ^0's makes spectators from those events appear forward peaked. Top right: $p_{missing}$ vs. mm($K^0\Lambda$) showing exclusive $K^0\Lambda$ events on the left, a band with extra pions on the right, and $K^0\Sigma^0$ events in the middle. Bottom right: Exclusive $K^0\Lambda$ events with proton spectators at the bottom and those having undergone final state interactions at the top.

it might be comparable to the KY case. As follows from the discussion in section 3.1.1, and as is shown in Figs. 2 and 3, the sensitivity could be considerably larger than for the differential cross section.

For the K^*Y channels, Capstick and Roberts predict that the two-star state $N[\frac{3}{2}^-]_1(2080)$ and the weakly established $N[\frac{1}{2}^-]_1(2090)$ state couple to $K\Lambda$ and $K^*\Lambda$ with comparable strength. It has been pointed out that the t-channel vector-meson exchange and the seagull term are proportional to the charge of the outgoing K^* meson [50]. Neutral K^* production,

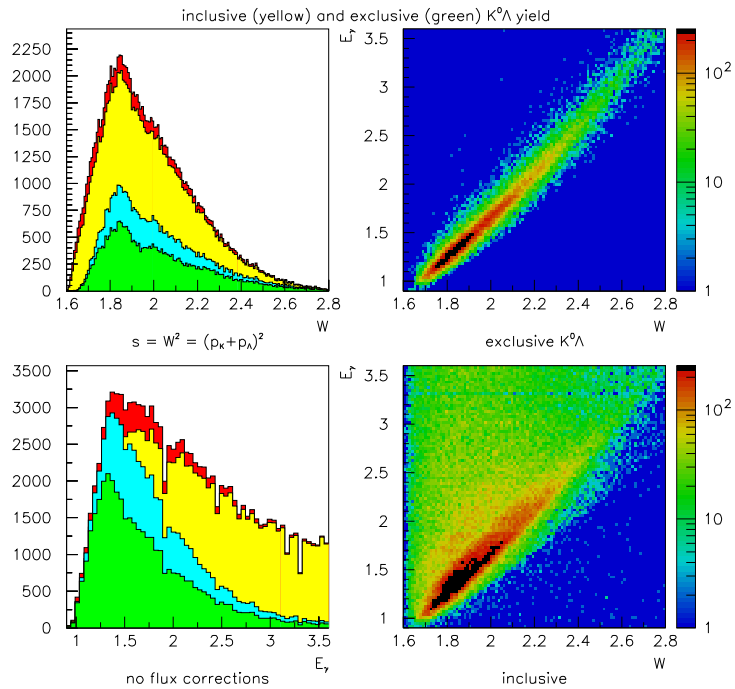

Figure 8: Preliminary yields from g10, not corrected for photon flux or CLAS acceptance as function of W calculated from the final state (top left) and E_γ (bottom left). Color coding: exclusive $K^0\Lambda$ (green), $K^0\Sigma^0$ (blue), and inclusive $K^0\Lambda$ with one proton detected and the spectator reconstructed (yellow) and with both protons detected (red). On the right are $W - E\gamma$ correlations for inclusive (bottom) and exclusive (top) $K^0\Lambda$ events.

where the t-channel background processes are suppressed, could thus provide a unique opportunity for N^* physics. A deuteron target is advantageous since it allows us to study the reaction $\vec{\gamma}n \to K^{*0}\Lambda \to K^+\pi^-\pi^-p$. As noted for the $K^+\Sigma^-(1385)$, this final state is well suited for CLAS. An exclusive measurement of the K^{*0} channel on the proton would, on the other hand, require the detection of either the neutron or π^0 from the decay of the Σ^+. Missing-mass techniques can be used for the cross section, but would not make it possible to obtain any polarization observables.

Currently, only a few KY^* cross section measurements have been made, all using a proton target, and there are no published photoproduction data on the neutron. There are, however, several N^* states, including the $N[\frac{1}{2}^-]_5(2070)$ (established in pion production) and

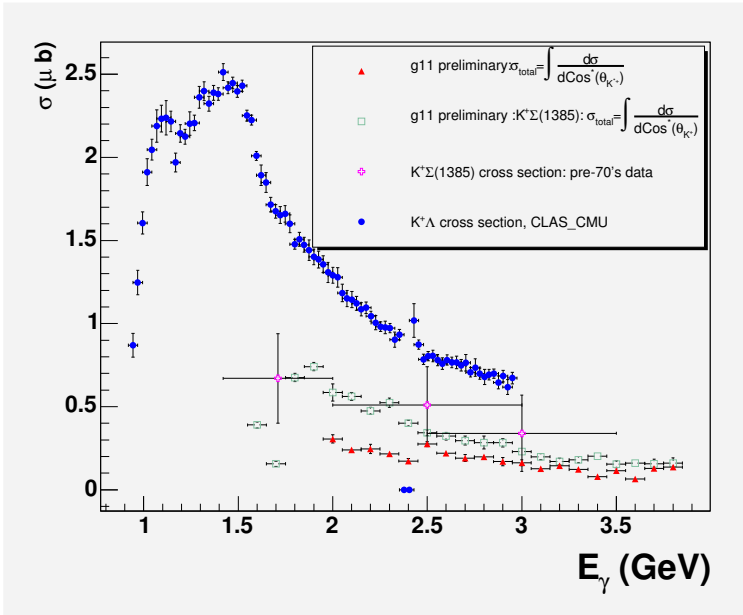

Figure 9: Total cross sections for the $K^*\Lambda$ and $K^+\Sigma^0(1385)$ channels compared with CLAS results for $K^+\Lambda$ photoproduction [46] and earlier $K^+\Sigma^0(1385)$ photoproduction data.

the $\Delta[\frac{3}{2}^-]_3(2145)$, that are predicted to couple strongly to KY^* channels, in particular the $K\Sigma(1385)$. The low-lying KY^* channels should also be important for lighter missing resonances, such as the $N[\frac{5}{2}^+]_2(1980)$ and $\Delta[\frac{3}{2}^+]_3(1985)$, which are below the K^*Y threshold. Preliminary differential cross section results for the $\gamma p \to K^+\Sigma^0(1385)$ reaction, obtained using the g11 data set, also show less contribution from t-channel processes than is the case for the $K^{*+}\Lambda$ channel.

To summarize, K^{*0} production in association with the Λ, as well as K^0Y^* production, seems more promising than the charged channels due to the suppression of t-channel non resonant background. The combination of a polarized photon beam and a deuteron target offers a unique opportunity to study N^* physics and perhaps discover missing nucleon resonances that would be hard to extract from proton data only.

3.3 Final-state interactions

3.3.1 Theory

The dominant processes in the photoproduction of kaons from the deuteron are shown in Fig. 10. The detailed expressions for the corresponding amplitudes are given in Ref. [25]. Here, we give only a brief sketch of the underlying physics and an update of the choice of the parameterization of the elementary amplitudes at lower energies. As an example, we consider the $\gamma d \to nK^+\Lambda$ reaction, but the extension to the $\gamma d \to pK^0\Lambda$ or $\gamma d \to nK^+\Lambda^*(1520)$ channels, as well as the Σ production channels, is straightforward.

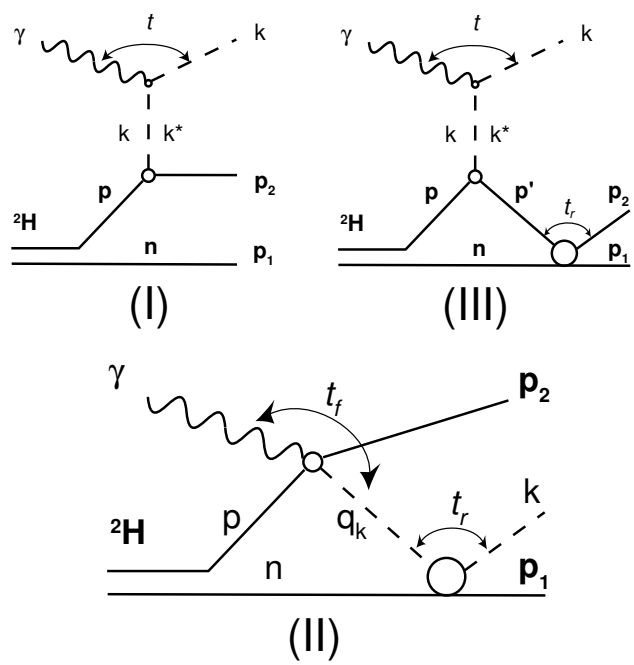

Figure 10: The relevant graphs in the $\gamma d \to nK^+\Lambda$ reaction. I: Quasi free kaon photoproduction. II: Kaon-nucleon rescattering. III: Lambda-nucleon rescattering.

Graph I represents the quasi free production of the K^+ on the proton, the neutron being a spectator. It dominates at low values of the spectator neutron momentum p_n, where the cross section takes the simple form [25, 51]:

$$\frac{d\sigma}{d\vec{p_n}d\Omega_k} = (1 + \beta_n \cos\theta_n)\rho(|\vec{p_n}|)\frac{d\sigma}{d\Omega_k}(\gamma p \to \Lambda K^+) \tag{6}$$

where $\beta_n = p_n/E_n$ and θ_n are the velocity and the angle of the spectator nucleon. This is nothing but the relation between the yield and the elementary cross section for the production of a kaon on a nucleon which moves with the velocity $-\vec{\beta_n}$. The number of target nucleons is $\rho(|\vec{p_n}|)d\vec{p_n}$, where $\rho(|\vec{p_n}|)$ is the momentum distribution of the proton in the deuteron (which we take from the Paris potential), while $(1 + \beta_n \cos\theta_n)$ is the flux of photons seen by the moving target nucleon.

When the neutron momentum increases, its momentum distribution decreases very quickly, and kaon-nucleon (graph II) as well as lambda-nucleon (graph III) rescatterings become dominant above $p_n \sim 300$ MeV/c. Since the available energy in each rescattering vertex is larger than the sum of the masses of the two particles which rescatter, both can be on-shell in the intermediate state. This induces a logarithmic singularity in each rescattering integral [25, 51]. Its effect is maximal on the cross section when the minimum momentum p_{min} of the spectator nucleon in the loop, for which the two particles which rescatter are on-shell, vanishes.

At the top of the corresponding peaks, the physical picture is the following. The Λ, or the K, is produced on a nucleon at rest and recatters on the second nucleon, also at rest in the deuteron, which then recoils with the observed momentum p_n. Here, the rescattering amplitude is on solid ground, since its depends on on-shell elementary matrix elements and relies on the low-momentum components of the deuteron wave function. This is a good place to study the interactions with nucleons of short-lived particles (such as the various hyperons) or to look for elusive narrow resonant states (*e.g.*, in the K^+n channel).

Figure 11 shows various observables which emphasize the kaon-nucleon rescattering sector. The real photon beam end point has been set to $E_\gamma = 2$ GeV. The panels show cross sections integrated over the various bins, within the CLAS fiducial acceptance. The top panels show the distribution of the minimum momentum $p_{min}(nK)$ of the spectator neutron, in the kaon-nucleon scattering loop, for which the pion can propagate on-shell. On the left, the cut $400 < n_R < 600$ MeV/c has been applied on the momentum p_n of the slow nu-

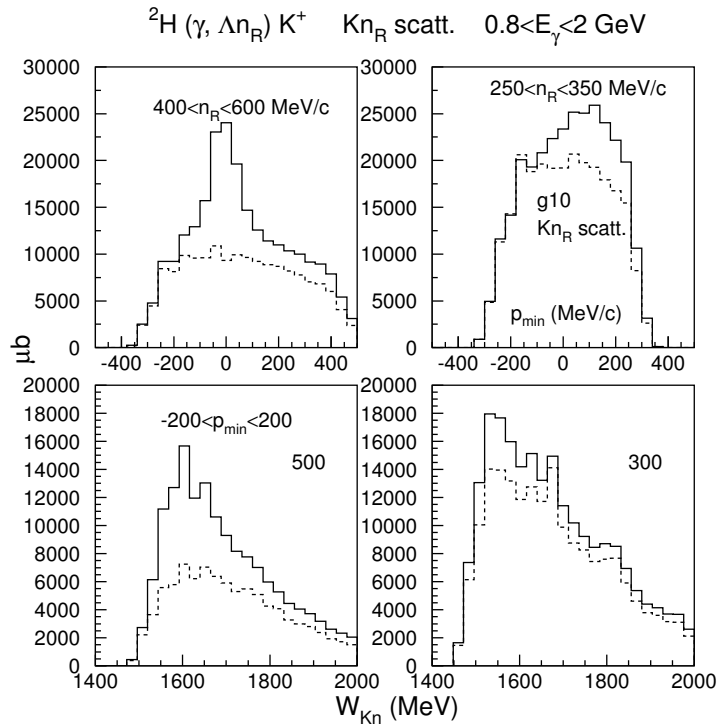

Figure 11: The kaon-nucleon rescattering sector.

cleon: the kaon-nucleon rescattering peak clearly appears at $p_{min} = 0$. On the right, the cut $250 < n_R < 350$ MeV/c has been applied; rescattering effects are small here, and the shape of the distribution reflects the kinematics and the detector acceptance. This is a good reference point that emphasizes the quasi free process. A further cut -200 $< p_{min}(nK) <$ 200 MeV/c has been applied in the bottom parts of Fig. 11, which emphasizes kaon-nucleon rescattering. The distribution of the mass W_{Kn} of the K^+n system is plotted on the left for the high recoil-momentum ($\sim$ 500 MeV/c) and on the right for the low recoil-momentum ($\sim$ 300 MeV/c) bands.

Figure 12 shows the same observables in the Λ-n rescattering sector. Now, the minimum momentum $p_{min}(n\Lambda)$ is the lowest value of the momentum of the spectator neutron for which the Λ can propagate on-shell in the Λ-N scattering loop. For the low recoil-momentum ($\sim$ 300 MeV/c) band (bottom right), strong S-wave rescattering enhances the distribution of the mass $W_{\Lambda n}$ of the Λn system near the Λ production threshold, but the quasi free process

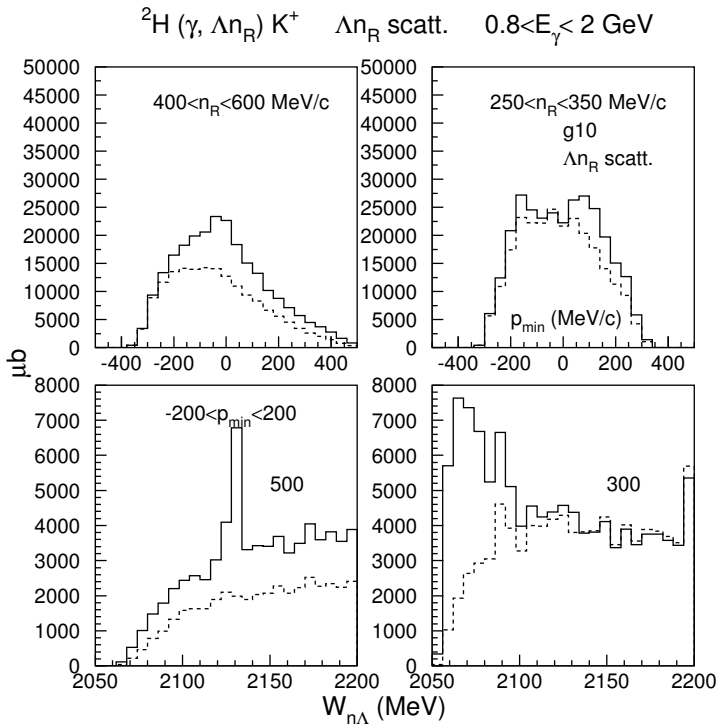

Figure 12: The lambda-nucleon rescattering sector.

contributes less for recoil-momenta above $\sim$ 300 MeV/c. For the high recoil-momentum ($\sim$ 500 MeV/c) bands (bottom left), CLAS acceptance suppresses the kinematical region near the Λ production threshold, but the quasi free process contribute less above. The cusp in the Λn scattering amplitude clearly appears at the Σ production threshold; it comes from the coupling between the Λ and the Σ channels.

Contrary to Ref. [25], where the high-energy description of the elementary scattering amplitudes has been used, here we use their low-energy phase-shift expansions. They have already led to a good accounting of kaon production in pp scattering [52, 53], but was not able to disentangle the Λ and Σ channels. This becomes possible with CLAS, which opens up the possibility to map out (for the first time) the hyperon - nucleon amplitudes in the vicinity of the Σ threshold and above. This is a strong constraint on the models that try to describe the interaction between hadrons.

In Fig. 11, Λn rescattering gives also a contribution below the K^+n rescattering peak.

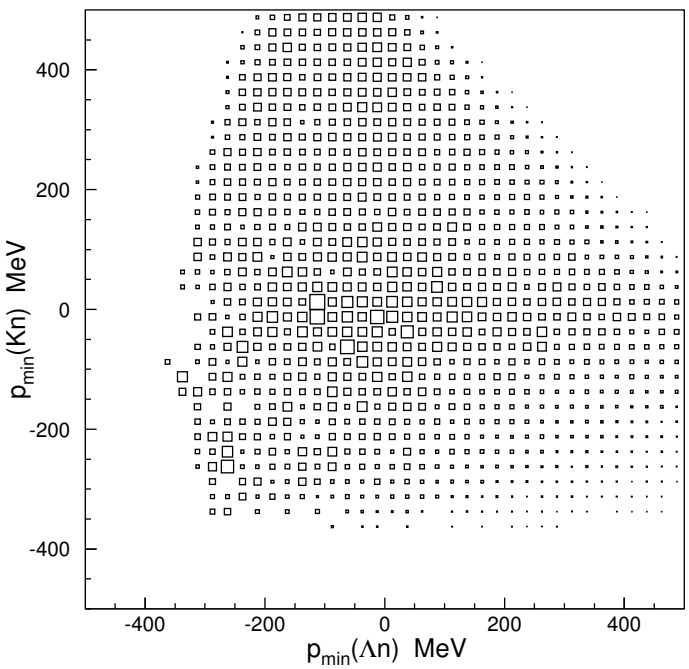

Figure 13: The joint distributions of the logarithmic singularities in the K^+n and Λn channels.

Also, K^+n rescattering gives a contribution under the Λn rescattering peak in Fig. 12. These contaminations can be removed by cutting out the overlapping region in the joint distribution of the rescattering singularities, which is shown in Fig. 13.

In all of these histograms, the model has been folded with the CLAS geometrical acceptance and physical cuts have been performed according to the method that is described in Ref. [25]. Only the geometrical fiducial cut of the kaon has been taken into account. This is the most important cut since it defines the momentum transfer between the photon and the kaon. Neither the in-flight decay of the kaon nor the $\Lambda \to p\pi^-$ decay have been taken into account; they are expected to lead to an almost constant overall reduction factor.

For the proposal, the model will be folded with the full acceptance and efficiency of CLAS. Besides normalization effects, the mass resolution effects will be important in trying to sort out the narrow structure of the cusp at the Σ production threshold. This effort is already underway: to provide a decent modeling of the physical background as well as the

size of the signal of a hypothetical pentaquark in the K^+n scattering channel for the g10 run.

3.3.2 Experiment

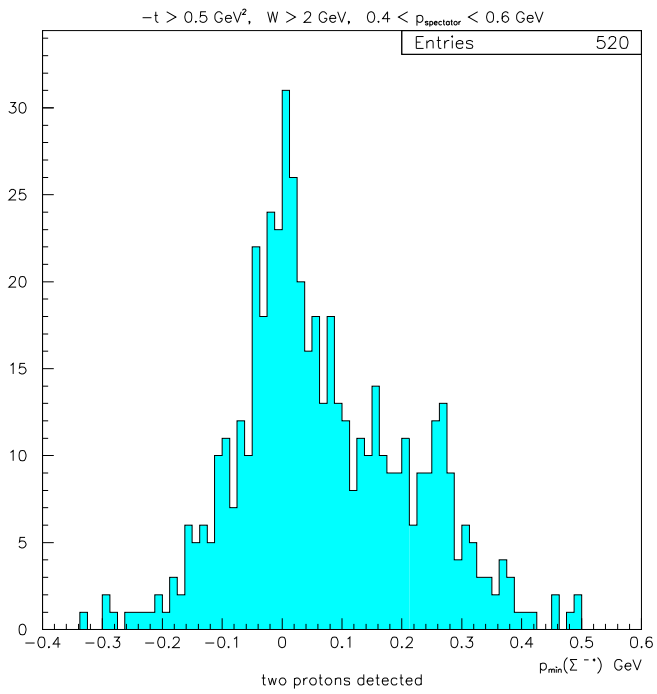

Figure 14: The $\Sigma^-(1385)$ rescattering peak can be seen in the minimum momentum $p_{min}(\Sigma p)$ that the spectator proton could have had before the rescattering (see section 3.3.1). The statistics in this histogram is small since -$t > 0.5$ GeV^2 and the detection of all final-state particles is required.

Unpolarized rescattering studies are currently in progress for the g10 data set using the Laget approach [25]. A preliminary p_{min} distribution showing a $\Sigma^-(1385)$ rescattering peak was presented at NSTAR 2005 [26], and is shown in Fig. 14. As predicted, there is a strong enhancement close to zero in the calculated minimum possible momentum of the "spectator" proton before the rescattering. The statistics in the plot is modest, since it was required that all five final-state particles be detected in CLAS, as well as that $-t > 0.5$ GeV^2 and $0.4 < p_{spectator} < 0.6$ GeV. What is important, however, is that it demonstrates that a rea-

sonably clean sample of events can be selected where the hyperon was rescattered on the spectator nucleon. In a similar way, events where the kaon was rescattered can be removed, which is made easier by the fact that the kaon peak has much less background under it. Studies of the less exotic, but perhaps more important Λ scattering are in progress. For all channels the statistics can be increased by looking at event topologies where either the spectator nucleon or the kaon is reconstructed from kinematics. The latter is especially attractive when dealing with the K^0, since only a third of them decay into $\pi^+\pi^-$. When not rescattered, the angular distribution for the kaons also tends to be strongly forward peaked, whereas that of true spectator protons is isotropic in the lab frame (see Fig. 7). While rescattering changes this picture somewhat, the acceptance for the protons remains significantly larger than that for both pions from the K_s^0 decay. Nevertheless, the number of events in the tail of the spectator nucleon momentum distribution will always be smaller than for the quasi free case (where the spectator momentum usually is below the detection threshold). More statistics would thus clearly allow a better determination of the cross sections and angular distributions for $Y - N$ scattering.

The ability to select rescattering events also opens up the possibility of studying polarization degrees of freedom. As predicted in [54], measurements on the free nucleon show a significant hyperon recoil polarization [32] at moderate momentum transfer (t). Rescattering effects in the deuteron are thus very well suited for investigating the $\vec{Y} - N$ interaction. Even without cuts on the reconstructed initial minimum spectator momentum, calculations demonstrate a high sensitivity of polarization observables to various interaction potentials and partial waves [27]. Obtaining good polarization data with a large-acceptance detector, allowing the study of exclusive processes, would thus open a new window on this field, not accessible through the study of bound hypernuclear states or experiments with unpolarized hyperon beams.

4 Experimental Parameters

4.1 Circular photon polarization

In this configuration, the optimal maximum photon energy is between 2.2 and 3.0 GeV. Our focus is at resonances well above the Λ threshold ($E_\gamma = 911$ MeV), and it is especially important to have sufficient statistics and good polarization for W between 1.8 and 2.0 GeV ($1.3 < E_\gamma < 1.7$ GeV). For circularly polarized photons, the polarization is highest when the difference between photon and electron energy is the smallest, but the higher energies are preferable for the study of K^* and Y^* channels. The experiment could thus run concurrently with G0 and still be a polarized extension of the g10 data set. Due to these considerations, no beam time will be requested for energies below 3 GeV. However, should low-energy beams become available, additional high-polarization data can be obtained closer to the Λ threshold.

The measurement of all of the exclusive processes proposed in this letter requires detection of at least one negative particle, typically the π^- from Λ decay. In order to maximize the acceptance, the data need to be taken with a low main torus field. This was done for half of the g10 data set, where a torus current of 2250 A was used. Preliminary analysis shows this setting to be satisfactory for the proposed channels. The somewhat higher maximum photon energy of g10 (3.6 GeV) has limited impact, since the number of events in this region is small, especially for the elementary reactions. The torus field can be optimized for each channel and maximum possible photon energy using Monte Carlo studies. If such a procedure leads to an adjustment, it will be presented in the final proposal. Another option that will be considered is to run with reversed polarity of the torus field, as was done for eg3. Since all channels require detection of at least as many positive as negative particles, however, this should not have a large impact on the acceptance.

During the g10 run period, a 24 cm long target was used, together with the old start counter. For the low-field part, the target was moved 25 cm upstream to further increase the acceptance for negative particles. In this experiment, we propose to use the 40 cm

target from g11 and the new start counter. A longer target is preferable because it allows a higher luminosity without increasing the event rate in the photon tagger. Moving the target upstream will also be considered in our acceptance Monte Carlo study. Such an arrangement will be especially interesting if it would allow the use of the inner calorimeter (IC) that was built for the e1-DVCS experiment. Its use would not only extend the acceptance for forward-going particles (such as the K_L^0), but, owing to its high granularity, would also make it possible to determine their angle accurately.

The trigger can be made rather restrictive. The optimum would be a level-1 two-sector trigger with a level-2 requirement of two charged tracks.

Since the proposed experiment uses equipment that is already available, the time for installation, testing, and commissioning be limited.

4.2 Linear photon polarization

The data with linear photon polarization will be taken in discrete points, each corresponding to a specific position of the relatively narrow coherent-photon peak. This gives the data a natural binning, reducing the systematic uncertainty. The photon energy and requested beam time for each point must, however, be determined independently (see our counting-rate estimate in section 4.3).

The optimum electron beam energy would be close to 6 GeV, or the maximum available. Approaching 6 GeV, however, one needs to consider the stability of the beam position on the diamond radiator, which is critical. The level of polarization depends on the energy of the electron beam. During the g8b run, which used a 4.5 GeV beam, over 90% was reached when the coherent peak was at 1.3 GeV and remained above 65% at 2.1 GeV. It is, however, important to note that even with a 3 GeV electron beam, more than 60% polarization can be achieved at 1.5 GeV. For data close to the Λ threshold, there will be significant polarization even at lower electron energies.

As in the case of the circularly polarized photons in section 4.1, a low torus field will

be required to increase the acceptance for negative particles. The optimal setting will be presented in the full proposal.

Since the coherent-bremsstrahlung photon peak covers only a few of the detector elements in the photon tagger, instead of the usual range from 20% to 95% of the electron beam energy, and is strongly collimated, the rate in the tagger is the limiting factor for the overall event rate. This limit is, however, less restrictive at lower electron energies. To ameliorate the rate problem, the use of the 40 cm long g11 target (which also was used for g8b) is critical. The rate limit in the tagger can also be increased by replacing some of the PM tube bases by faster ones. This is a low-cost upgrade option.

When using a linearly polarized beam, the trigger conditions could in principle be as restrictive as in the case of circular polarization. However, since the rate is limited by the tagger, there is no need to require more than two tracks. It would also be possible to share the beam time with experiments that need single-track events without causing a major impact on the total beam-time request.

With the possible exception of exchanging some of the PM tube bases in the photon tagger, this experiment does not require any new equipment. Even if the tubes should be replaced, this is a straightforward procedure that would not require much time for installation, testing, and commissioning.

4.3 Counting-rate estimate

Since the need for statistics depends on the reaction channel, the main purpose of this letter is to outline the options. The final proposal will include a more specific beam-time request based on feedback from the PAC and simulations using new event generators. In general, though, more statistics will be available for the elementary processes, and less for the K^* and Y^* channels. The exact ratios do, however, depend on the specific channel. For instance, only one K^0 out of three decays to $\pi^+\pi^-$. As seen in g10, the number of $K^+\Sigma^-(1385)$ events will thus be within a factor of two of those in the $K^0\Lambda$ channel, with the exact value

somewhat dependent on the maximum photon energy. Studies of final-state interactions also need more beam time for comparable statistics. A detailed counting-rate estimate, based on Monte Carlo simulations, will be given in the final proposal.

For circularly polarized photons, the request would be made nominally for a maximum photon energy of 3 GeV, but as discussed in section 4.1, there is an option to obtain part of the data at a lower energy. With a longer target and upgraded DAQ, the count rate can be somewhat higher than for g10. We estimate that ten billion triggers could be accumulated in about six weeks.

The linearly polarized photon data would be taken in photon energy intervals of 0.2 GeV, *i.e.*, the energy range below the coherent edge at which flux and polarization are roughly constant. Data are needed from 1.05 GeV, corresponding to a W of 1.69 GeV. This is the threshold for Σ production and the predicted peak for the total $K^0\Lambda$ cross section. The first four bins, up to $E_\gamma = 1.65$ GeV, would cover the elementary KY reactions and low-t final-state interactions. These data could be taken with an electron beam of comparatively low energy (3 GeV and below). For the K^* and Y^* channels, we propose four additional points, covering a range in W between 2.1 and 2.4 GeV. Here it would be preferable to have an electron beam of higher energy (4.5 to 5.5 GeV). Using the g8b experiment as a guideline, we estimate that we could take at least one billion triggers per week.

Finally, an important aspect of the proposed experiment that we want to stress is the flexibility in the allocation of beam time for different energies and polarizations. As a consequence, it can run concurrently with low-energy experiments in other halls.

References

[1] S. Capstick, Phys. Rev. D **34**, 2809 (1986).

[2] R.E. Cutkosky and R.E. Hendrick, Phys. Rev. D **16**, 2902 (1977).

[3] G. Penner and U. Mosel, Phys. Rev. C **66**, 055212 (2002).

[4] A. Waluyo, PhD thesis, The George Washington University, Washington, DC (2005).

[5] H. Yamamura *et al.*, Phys. Rev. C **61**, 014001 (1999).

[6] F.X. Lee, T. Mart, C. Bennhold, H. Haberzettl, and L.E. Wright, Nucl. Phys. **A695**, 237 (2001).

[7] T. Mart, C. Bennhold, H. Haberzettl, and L. Tiator, Kaon MAID 2000. http://www.kph.uni-mainz.de/MAID/kaon/kaonmaid.html

[8] J.C. David, C. Fayard, G.H. Lamot, and B. Saghai, Phys. Rev. C **53**, 2613 (1996).

[9] S. Janssen, J. Ryckebusch, W. Van Nespen, D. Debruyne, and T. Van Cauteren, Eur. Phys. J. **A11**, 105 (2001).

[10] S. Janssen, J. Ryckebusch, D. Debruyne, and T. Van Cauteren, Phys. Rev. C **65**, 015201 (2001).

[11] S. Janssen, J. Ryckebusch, D. Debruyne, and T. Van Cauteren, Phys. Rev. C **66**, 035202 (2002).

[12] S. Capstick and W. Roberts, Phys. Rev. D **58**, 074011 (1998).

[13] R. Koniuk and N. Isgur, Phys. Rev. D **21**, 1868 (1980).

[14] F.J. Klein *et al.*, Nucl. Intrum. Methods **A** (submitted, 2005).

[15] F.J. Klein *et al.*, JLab Hall B approved experiment E-02-112. http://www.jlab.org/exp_prog/proposals/02/PR02-112.ps

[16] T. Mart, C. Bennhold, and C.E. Hyde-Wright, Phys. Rev. C **51**, 1074(R) (1995).

[17] T. Mart and C. Bennhold, Phys. Rev. C **61**, 012201(R) (1999)

[18] C. Bennhold, A. Waluyo, H. Haberzettl, T. Mart, G. Penner, and U. Mosel, nucl-th/0008024 (2000).

[19] V. Shklyar, H. Lenske, and U. Mosel, Phys. Rev. C **72**, 015210 (2005).

[20] B. Saghai, nucl-th/0105001 (2001).

[21] S. Capstick, Phys. Rev. D **46**, 2864 (1992).

[22] X. Li, L.E. Wright, and C. Bennhold, Phys. Rev. C **45**, 2011 (1992).

[23] O. Maxwell, Phys. Rev. C **69**, 034605 (2004).

[24] A. Salam and H. Arenhövel, Phys. Rev. C **70**, 044008 (2004).

[25] J.-M. Laget, nucl-th/0507035.

[26] R. Davis, P. Nadel-Turoński, and B.L. Berman, poster presented at NSTAR 2005. http://www.jlab.org/~turonski/rebecca.ppt

[27] K. Miyagawa, T. Mart, C. Bennhold, and W. Glöckle, preprint (2005).

[28] Jefferson Lab PAC 28, (2005).

[29] M.Q. Tran, Phys. Lett. **B445**, 20 (1998).

[30] K.-H. Glander *et al.*, Eur. Phys. J. **A19**, 251 (2004).

[31] J.W.C. McNabb *et al.*, Phys. Rev. C **69**, 042201(R) (2004). http://www.jlab.org/Hall-B/general/thesis/mcnabb/

[32] R. Bradford *et al.*, nucl-ex/0509033, submitted to Phys. Rev. C (2005).

[33] R. Schumacher *et al.*, JLab Hall B completed experiment E-89-004. http://www.jlab.org/exp_prog/proposals/89/PR89-004.pdf

[34] B. Mecking *et al.*, JLab Hall B completed experiment E-89-045. http://www.jlab.org/exp_prog/proposals/89/PR89-045.pdf

[35] A. Lima, J. Langheinrich, and B.L. Berman, CLAS Analysis Note (submitted, 2005).

[36] I. Niculescu, nucl-ex/0108013 (2005).

[37] K. Hicks *et al.*, JLab Hall B completed experiment E-03-113. http://www.jlab.org/exp_prog/proposals/03/PR03-113.ps

[38] P. Nadel-Turoński and B.L. Berman, g10 analysis in progress (2005).

[39] D. Husmann and W.J. Schwille, Phys. Bl. **44**, 40 (1988).

[40] T. Nakano *et al.*, Nucl. Phys. **A684**, 71c (2001).

[41] R.G.T. Zegers *et al.*, Phys. Rev. Lett. **91**, 092001 (2003).

[42] S. Eidelman *et al.*, Phys. Lett. **B592**, 1 (2004).

[43] T. Feuster and U. Mosel, Phys. Rev. C**58**, 457 (1998).

[44] R.M. Davidson and R. Workman, Phys. Rev. C **63**, 025210 (2001).

[45] M. Dugger *et. al.*, Phys. Rev. Lett. **89**, 222002 (2002).

[46] J.W.C. McNabb, Ph.D. thesis, Carnegie Mellon University, Pittsburg, PA (2003).

[47] T.P. Vrana, S.A. Dytman, and T.S.H. Lee, Phys. Rep. **328**, 181 (2000).

[48] G. Knöchlein, D. Dreschsel, and L. Tiator, Z. Phys. **A352** (1995).

[49] L. Guo and D. Weygand, contributed talk at NSTAR 2005.
http://www.jlab.org/~lguo/nstar/sigma_nstar.ppt

[50] Q. Zhao, J.S. Al-Khalili, and C. Bennhold, Phys. Rev. C **64**, 052201 (2001).

[51] J.-M. Laget, Phys. Rep. **69**, 1 (1981).

[52] J.-M. Laget, Phys. Lett. **B259**, 24 (1991).

[53] J.-M. Laget, J. Korean Phys. Soc. **26**, S244 (1993).

[54] M. Guidal, J.-M. Laget, and M. Vanderhaegen, Nucl. Phys. **A627**, 645 (1997).